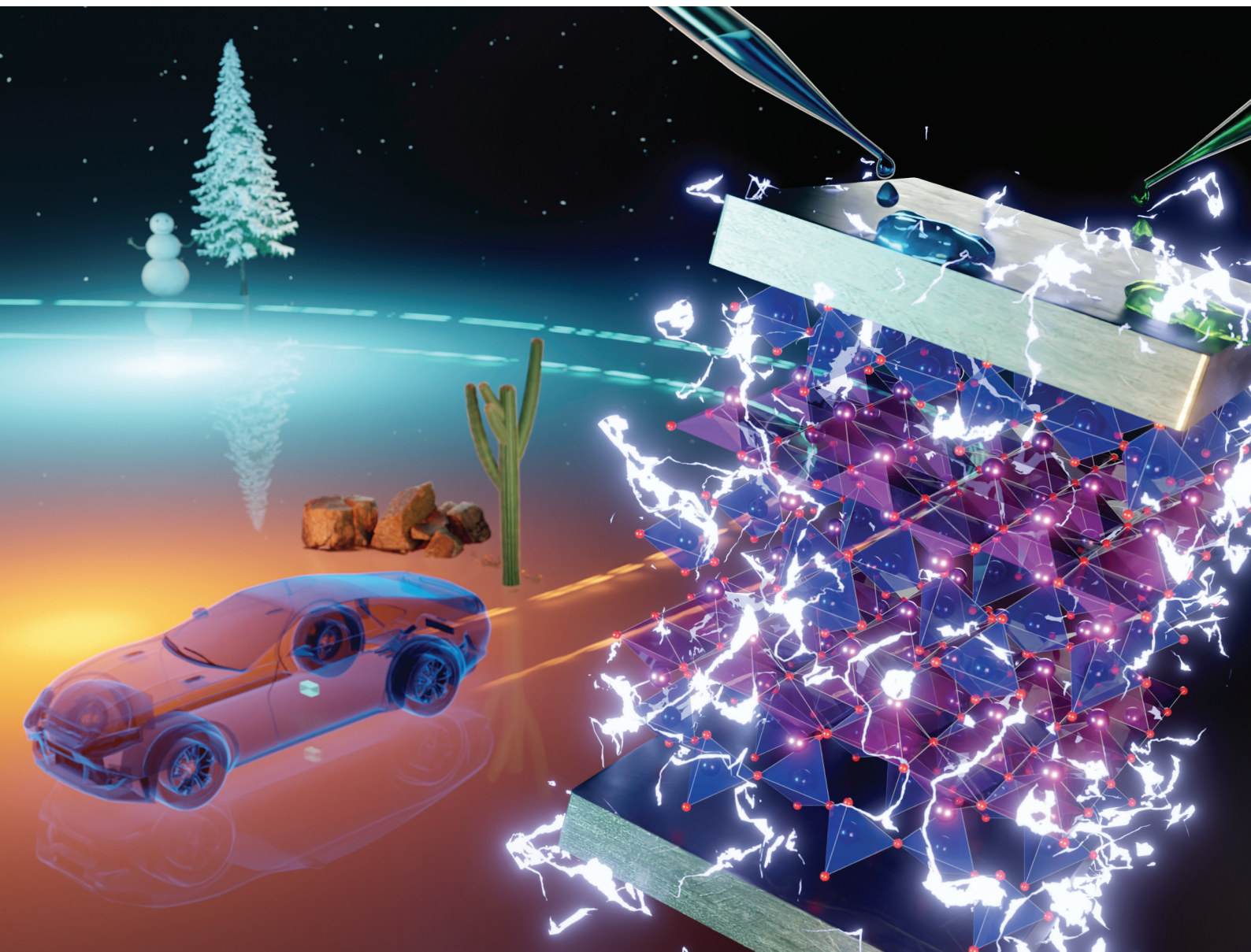


Dalton Transactions

An international journal of inorganic chemistry

rsc.li/dalton



ISSN 1477-9226

PAPER

Manabu Hagiwara *et al.*

Improving the dielectric temperature stability of Bi_2SiO_5 -based ceramics through the spontaneous formation of paraelectric-ferroelectric nanocomposite structures

Cite this: *Dalton Trans.*, 2025, **54**, 13869

Improving the dielectric temperature stability of Bi₂SiO₅-based ceramics through the spontaneous formation of paraelectric–ferroelectric nanocomposite structures

Yoji Yasumoto,^a Taro Kuwano,^b Hiroki Taniguchi,^c Shinobu Fujihara^a and Manabu Hagiwara^{id}*^a

The substitution of a portion (~3%) of Bi³⁺ in ferroelectric Bi₂SiO₅ ceramics with La³⁺ induces a paraelectric phase and stabilizes the dielectric permittivity by eliminating the ferroelectric–paraelectric phase transition. However, the non-negligible negative temperature dependence of the permittivity remains an issue for practical applications in capacitors, resonators, and antennas. Herein, we show that the additional substitution of Si⁴⁺ with Ge⁴⁺ in paraelectric (Bi_{0.97}La_{0.03})₂SiO₅ can substantially improve its dielectric temperature stability. Ceramic samples with compositions of (Bi_{0.97}La_{0.03})₂Si_{1-x}Ge_xO₅ with *x* up to 0.3 were prepared via a sol–gel process and subsequent low-temperature sintering below 720 °C. The incorporation of Ge stabilized the ferroelectric phase with an elevated Curie temperature, leading to the spontaneous formation of a paraelectric–ferroelectric nanocomposite structure. The fraction of the ferroelectric phase increased from 0% at *x* = 0 to 53% at *x* = 0.3. Because of the negative and positive temperature dependence of the paraelectric and ferroelectric phases, respectively, the sample with *x* = 0.2 exhibited a dielectric permittivity over 50 with a small temperature coefficient of -70 ± 50 ppm °C⁻¹ in a temperature range from -55 to 125 °C. The ceramics also showed a paraelectric-like linear polarization response under electric fields up to 280 kV cm⁻¹.

Received 12th June 2025,
Accepted 23rd July 2025

DOI: 10.1039/d5dt01380a

rsc.li/dalton

Introduction

Dielectric ceramics with a high temperature stability of the dielectric permittivity (ϵ_r) are essential for a wide range of applications, including Class I (temperature compensating) multilayer ceramic capacitors (MLCCs) for electronics devices as well as resonators and antennas for wireless communication systems.^{1,2} In particular, the market for Class I MLCCs used in power electronics systems for electric vehicles is growing rapidly due to their high temperature and high voltage compatibility.³ Paraelectric CaZrO₃ is commonly used in such MLCCs, but its ϵ_r is as low as 30.¹ Thus, the development of dielectric ceramics with higher and temperature-stable ϵ_r is required for the downsizing and weight reduction of power electronic circuits, contributing to the reduction of greenhouse gas emissions. Dielectric

ceramics with $\epsilon_r > 50$ and near-zero temperature dependence of ϵ_r are also increasingly demanded for use in resonators for smartphone base stations.⁴

The temperature dependence of dielectric materials is often evaluated using the temperature coefficient of capacitance (TCC), which is calculated as follows:⁵

$$\text{TCC} = \frac{C_T - C_{25}}{C_{25} \times (T - 25)} \times 10^6 \text{ (ppm } ^\circ\text{C}^{-1}) \quad (1)$$

where *T* is the temperature in °C, and *C_T* and *C₂₅* are the capacitance values at *T* and 25 °C (base temperature), respectively. For example, the C0G specification for Class I MLCCs, which is the most stringent temperature stability standard, requires zero TCC with a tolerance of ± 30 ppm °C⁻¹ over a temperature range from -55 to 125 °C.¹ For application in microwave devices such as resonators and antennas, the temperature coefficient of the resonant frequency (TCF) is also commonly used, which is given as $\text{TCF} = -(\text{TCC} + \alpha_L)/2$, where α_L is the linear thermal expansion coefficient.² As dielectric ceramics generally exhibit low α_L (around +10 ppm °C⁻¹), TCC determines the TCF in most dielectric ceramics.⁶ The possibility of sintering at low temperatures is also an important factor in many applications because low sintering tempera-

^aDepartment of Applied Chemistry, Faculty of Science and Technology, Keio University, 3-14-1 Hiyoshi, Kohoku-ku, Yokohama 223-8522, Japan.

E-mail: hagiwara@applied.keio.ac.jp

^bDepartment of Materials Science and Engineering, Institute of Science Tokyo, 4259 Nagatsuta-cho, Midori-ku, Yokohama, 226-8501, Japan

^cDepartment of Physics, Nagoya University, Furo-cho, Chikusa-ku, Nagoya 464-8602, Japan



tures enable the co-firing of ceramics with low-melting metal electrodes such as Ag and Al, thereby reducing the material cost of devices.^{7,8}

Recently, we reported that La-substituted Bi_2SiO_5 synthesized *via* a sol-gel process can be sintered at 700 °C and possesses relatively high and temperature-stable dielectric permittivity ($\epsilon_r = 59$ at 25 °C).⁹ Bi_2SiO_5 is a unique and unconventional ferroelectric oxide with spontaneous polarization occurring because of the twisting of one-dimensional chains of corner-sharing SiO_4 tetrahedra [Fig. 1(a) and (c)].¹⁰ Pristine Bi_2SiO_5 transforms from a ferroelectric (monoclinic Cc) phase to a paraelectric (orthorhombic $Cmcm$) phase at the Curie temperature (T_C) of approximately 400 °C upon heating, resulting in a strong positive temperature dependence of ϵ_r .^{10,11} The substitution of a portion (~3%) of Bi^{3+} in Bi_2SiO_5 with La^{3+} perturbs the SiO_4 chains, transforming the ferroelectric phase to another paraelectric phase with the tetragonal $I4/mmm$ symmetry [Fig. 1(b) and (d)].^{12,13} This structural change eliminates the dielectric peak, greatly improving the temperature stability of ϵ_r while maintaining a relatively high ϵ_r .^{9,13} However, La-substituted Bi_2SiO_5 ceramics still have negative TCCs (approximately $-400 \text{ ppm } ^\circ\text{C}^{-1}$),⁹ so further improvement of the dielectric temperature stability is essential for practical applications.

The general strategy for improving the temperature stability (TCC or TCF) of dielectric ceramics with low to medium ϵ_r involves two main approaches: the preparation of composites and the formation of solid solutions.⁶ The first approach requires two dielectric materials with temperature coefficients of opposite signs and very different crystal structures. For example, spinel-type ZnAl_2O_4 (TCF = $-79 \text{ ppm } ^\circ\text{C}^{-1}$) and rutile-type TiO_2 (TCF = $+423 \text{ ppm } ^\circ\text{C}^{-1}$) can be sintered into composite ceramics exhibiting $\epsilon_r = 20$ with TCF close to zero at 30% TiO_2 content.¹⁴ This approach can only be used when the two

dielectric materials do not react with each other. As Bi_2SiO_5 is a metastable phase in the Bi_2O_3 - SiO_2 system,¹⁵ the sintering of Bi_2SiO_5 in the presence of another dielectric material may easily cause the decomposition of the Bi_2SiO_5 phase. Therefore, the conventional composite formation approach is not suitable for Bi_2SiO_5 -based dielectric ceramics.

In the second approach (solid solution formation), two or more end members with the same crystal structure but TCC or TCF of opposite signs are employed. For example, solid solution ceramics composed of perovskite-type CaTiO_3 (TCF = $800 \text{ ppm } ^\circ\text{C}^{-1}$) and NdAlO_3 (TCF = $-33 \text{ ppm } ^\circ\text{C}^{-1}$), namely $\text{Ca}_{1-x}\text{Nd}_x\text{Ti}_{1-x}\text{Al}_x\text{O}_3$, show a near-zero TCF at $x = 0.3$.¹⁶ This approach has been widely used with perovskite-type oxides because of the large number of such materials with TCC or TCF of opposite signs. However, no materials with positive TCC are known to form solid solutions with La-substituted Bi_2SiO_5 . For this reason, the solid solution approach is also not applicable to Bi_2SiO_5 -based ceramics, thus requiring the development of a novel method for controlling the TCC.

Herein, we propose a unique method to improve the TCC of Bi_2SiO_5 -based ceramics: the spontaneous formation of nano-composite structures of ferroelectric and paraelectric phases. As the ferroelectric Cc phase has a positive TCC whereas the paraelectric $I4/mmm$ phase has a negative TCC, the composite formation between these phases brings TCC toward zero. To prepare this composite, we simultaneously substituted Bi^{3+} and Si^{4+} in Bi_2SiO_5 with La^{3+} and Ge^{4+} , respectively. Bi_2GeO_5 is a structural analog of Bi_2SiO_5 , and *ab initio* calculations suggest that the stability of the ferroelectric phase relative to the high temperature paraelectric phase in Bi_2GeO_5 is higher than that in Bi_2SiO_5 .¹⁷ Thus, the substitution of Si^{4+} with Ge^{4+} is expected to stabilize the ferroelectric phase of Bi_2SiO_5 and shift T_C to higher temperatures. At the same time, the doping

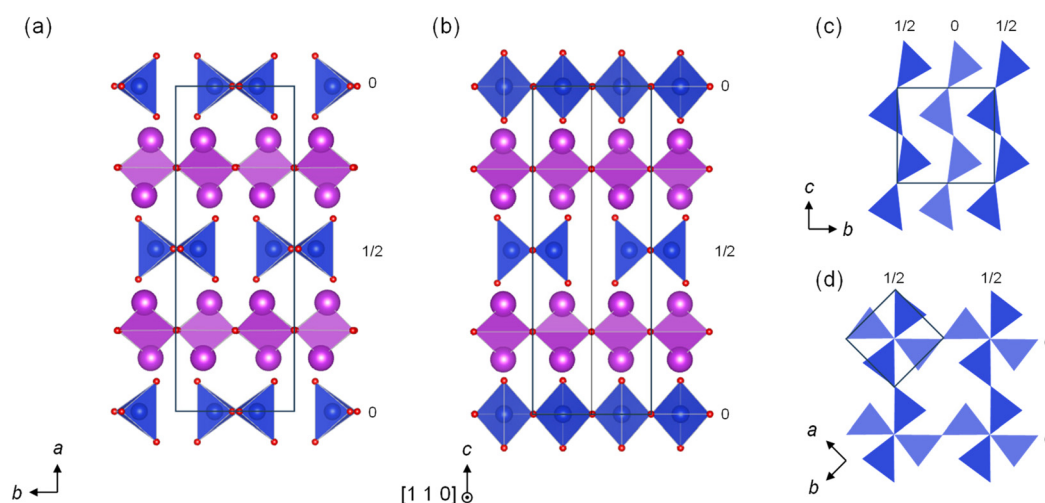


Fig. 1 (a and b) Schematic illustrations of the crystal structures of (a) the monoclinic Cc phase of Bi_2SiO_5 , viewed along the c -axis, and (b) the tetragonal $I4/mmm$ phase (local ordered description) of La-substituted Bi_2SiO_5 , viewed along the $[1\ 1\ 0]$ direction.^{10,13} Purple, blue, and red spheres represent Bi (and La), Si, and O atoms, respectively. The solid-line squares represent the unit cells. (c and d) Connectivity of SiO_4 tetrahedra in the (c) monoclinic phase (viewed along the c -axis) and (d) tetragonal phase (viewed along the c -axis). Note that the long-range connectivity of the SiO_4 network in the tetragonal phase is disordered.¹³



of La^{3+} into Bi^{3+} sites breaks the long-range ferroelectric order, leading to a competition between the stabilities of the ferroelectric and paraelectric states. In this study, Bi_2SiO_5 ceramics simultaneously substituted with La (3 mol%) and Ge (0–30 mol%) are prepared *via* a previously developed sol-gel process, and their crystalline phases and microstructures were investigated. The results show that the sintering of co-substituted ceramics results in the spontaneous formation of a nanocomposite structure with a TCC of $-70 \pm 50 \text{ ppm } ^\circ\text{C}^{-1}$ and $\epsilon_r > 50$ in the temperature range of from -55 to 125 °C.

Experimental

Sample preparation

Bi_2SiO_5 ceramics co-substituted with La and Ge, with nominal compositions of $(\text{Bi}_{0.97}\text{La}_{0.03})_2\text{Si}_{1-x}\text{Ge}_x\text{O}_5$ ($x = 0, 0.1, 0.2, \text{ and } 0.3$), were synthesized *via* a sol-gel process reported in our previous works.^{9,11} The La content was fixed at 3 mol% because Bi_2SiO_5 substituted with only La changes to the paraelectric phase at this La concentration.⁹ Tetraethyl orthosilicate $\text{Si}(\text{OC}_2\text{H}_5)_4$ (TEOS; 99.9%, Kanto Chemical Co., Inc.), tetraethyl orthogermanate $\text{Ge}(\text{OC}_2\text{H}_5)_4$ (TEOG; 99.999%, Kojundo Chemical Laboratory Co., Ltd), bismuth nitrate pentahydrate $(\text{Bi}(\text{NO}_3)_3 \cdot 5\text{H}_2\text{O}; 99.9\%$, FUJIFILM Wako Pure Chemical Corporation), and lanthanum nitrate hexahydrate $(\text{La}(\text{NO}_3)_3 \cdot 6\text{H}_2\text{O}; 99.9\%$, FUJIFILM Wako Pure Chemical Corporation) were used as starting materials without further purification.

TEOS [$6.0 \times (1 - x)$ mmol] was dissolved in a mixture of water (1.0 mL) and ethanol (1.3 mL), followed by the addition of citric acid (0.1 g) as a catalyst for hydrolysis. The solution was stirred at room temperature for 15 min to prehydrolyze TEOS, after which ethanol (4.7 mL) was added to prepare a Si solution. Separately, TEOG ($6.0 \times x$ mmol) was dissolved in ethanol (6.00 mL) to prepare a Ge solution. In addition, $\text{Bi}(\text{NO}_3)_3 \cdot 5\text{H}_2\text{O}$ (11.64 mmol) and $\text{La}(\text{NO}_3)_3 \cdot 6\text{H}_2\text{O}$ (0.36 mmol) were dissolved in a mixture of L-lactic acid (3.2 mL) and water (7.8 mL) at 60 °C. The resulting solution was cooled to room temperature to prepare a Bi-La solution. The Si and Ge solutions were added dropwise to the Bi-La solution under stirring, followed by additional stirring for 30 min at room temperature. The resulting transparent solution was gelatinized and dried at 65 °C to obtain a xerogel. The xerogel was pulverized in a mortar and pyrolyzed at 300 °C for 1 h under airflow, followed by calcination at 500 °C for 30 min in air to obtain $(\text{Bi}_{0.97}\text{La}_{0.03})_2\text{Si}_{1-x}\text{Ge}_x\text{O}_5$ fine powders.

The obtained powders were ball-milled in ethanol for 24 h, after which poly(vinyl alcohol) (2 wt%) and CH_3COOLi (4 mol%) were added as a binder and a sintering aid, respectively, and the mixture was uniaxially pressed at 100 MPa into 6 mm (diameter) pellets, followed by cold isostatic pressing at 150 MPa. The green bodies were heat-treated at 400 °C for 1 h in air to remove the binder, followed by sintering at 680–720 °C for 1 h in air to obtain $(\text{Bi}_{0.97}\text{La}_{0.03})_2\text{Si}_{1-x}\text{Ge}_x\text{O}_5$ ceramics. The short holding time was essential to suppress the decomposition of the Bi_2SiO_5 -type phase during sintering.

Characterization

The density of the ceramic samples was measured using Archimedes' method. The crystal phases of the samples were determined *via* X-ray diffraction (XRD) analysis using a Bruker D8 ADVANCE diffractometer with a Cu $K\alpha$ radiation source. The XRD patterns of the ceramic samples were analyzed using the Rietveld refinement software RIETAN-FP¹⁸ to determine the phase contents. The crystallite sizes of the Bi_2SiO_5 -type phases were estimated by applying the Halder-Wagner method to the diffraction angle dependence of the profile parameters refined by the Rietveld method, using the algorithm implemented in the RIETAN-FP program. The crystallite sizes obtained by such a method are expected to carry an uncertainty of at least ± 10 –20%.¹⁹ The microstructure of the samples was observed using field-emission scanning electron microscopy (FE-SEM) using a JEOL JSM-7600F microscope. The elemental distribution in sample particles was studied by high-angle annular dark-field scanning transmission electron microscopy-energy dispersive spectroscopy (HAADF-STEM-EDS) using an FEI Tecnai Osiris microscope.

To investigate their dielectric properties, the ceramic samples were polished to a thickness of approximately 0.7 mm, and Au electrodes were sputtered onto both the bottom and top surfaces. The temperature dependence of the capacitance and dielectric loss ($\tan \delta$) were measured in the temperature range from -170 to 450 °C using an Agilent 4284A precision LCR meter equipped with a Linkam THMS600 temperature controller. TCC was calculated based on the measured temperature dependence of capacitance using eqn (1). Capacitance was converted to permittivity using the sample dimensions measured at room temperature. To measure the polarization (P)–electric field (E) loops, the ceramic samples were polished to a thickness of approximately 0.15 mm, after which an Au electrode with a diameter of 1 mm was sputtered onto the top surface and the bottom surface was completely sputter-coated with Au. The P – E loops were measured using a TOYO Corp. FCE10-B ferroelectric characterization system equipped with a Matsusada Precision Inc. HEOPT-10B10 high-voltage amplifier.

Results and discussion

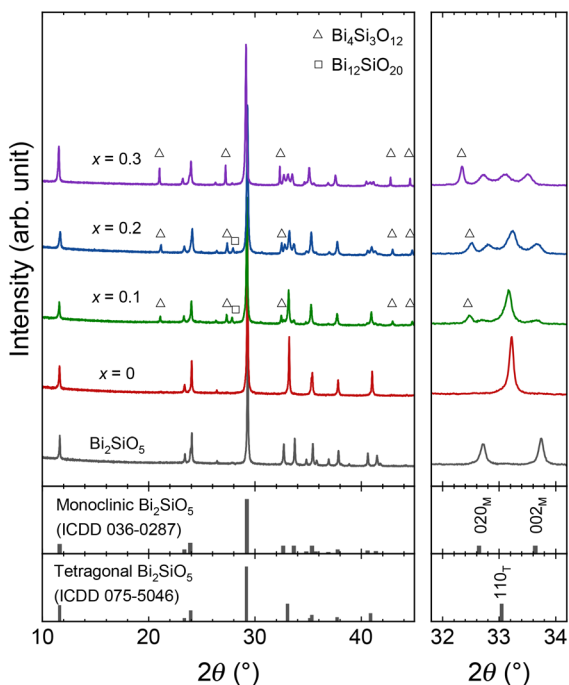
As Bi_2SiO_5 is a metastable phase, it readily decomposes into $\text{Bi}_4\text{Si}_3\text{O}_{12}$ and $\text{Bi}_{12}\text{SiO}_{20}$ at temperatures above 600 °C.^{12,15,20} Although the addition of lithium acetate promotes the densification of Bi_2SiO_5 and the incorporation of a small amount of La^{3+} at the Bi^{3+} site of Bi_2SiO_5 retards thermal decomposition, the sintering of Bi_2SiO_5 -based materials remains very challenging.^{9,11} Thus, herein, the sintering temperature for $(\text{Bi}_{0.97}\text{La}_{0.03})_2\text{Si}_{1-x}\text{Ge}_x\text{O}_5$ ceramics was optimized for each composition ($x = 0, 0.1, 0.2, \text{ and } 0.3$) to balance the sintered density and the amount of secondary phases. The optimal sintering temperatures and the relative densities of the resulting ceramics are listed in Table 1. Although the samples are not perfectly densified, the relative densities of all samples are above 80%.



Table 1 The optimal sintering temperature and the relative density of $(\text{Bi}_{0.97}\text{La}_{0.03})_2\text{Si}_{1-x}\text{Ge}_x\text{O}_5$ ceramics ($x = 0, 0.1, 0.2, \text{ and } 0.3$)

x	Sintering temperature ($^{\circ}\text{C}$)	Relative density (%)
0	720	91.4
0.1	700	91.0
0.2	680	82.2
0.3	700	84.9

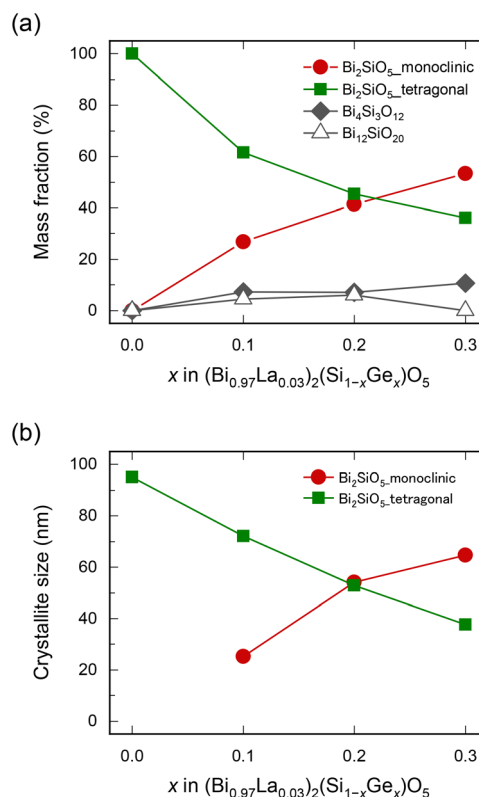
Fig. 2 shows the XRD patterns of the $(\text{Bi}_{0.97}\text{La}_{0.03})_2\text{Si}_{1-x}\text{Ge}_x\text{O}_5$ ceramics sintered at the optimum temperatures. For comparison, the XRD pattern for pristine Bi_2SiO_5 prepared *via* a similar sol-gel process is also shown.⁹ The diffraction peaks of pristine Bi_2SiO_5 were assigned to the monoclinic (Cc) structure, which is the ferroelectric phase with the spontaneous polarization caused by the twisting of SiO_4 chains.¹⁰ At the same time, the sample doped only with 3 mol% La ($x = 0$) exhibits a paraelectric tetragonal ($I4/mmm$) structure, consistent with previous reports.^{9,12,13} This is because the substitution of Bi^{3+} with La^{3+} induces the disordering of SiO_4 chains.¹³ The diffraction peaks for the $x = 0.1$ sample were mainly assigned to the tetragonal phase, with weak additional peaks at lower and higher angles relative to the tetragonal 1 1 0 peak assigned to the 0 2 0 and 0 0 2 lattice planes of the ferroelectric monoclinic phase. The intensity of the diffraction peaks of the monoclinic phase increases with Ge content, whereas peaks of the tetragonal phase are observed even at $x = 0.3$, indicating that the monoclinic and tetragonal phases coexist in $(\text{Bi}_{0.97}\text{La}_{0.03})_2\text{Si}_{1-x}\text{Ge}_x\text{O}_5$ over a

**Fig. 2** XRD patterns of the $(\text{Bi}_{0.97}\text{La}_{0.03})_2\text{Si}_{1-x}\text{Ge}_x\text{O}_5$ ceramics with $x = 0, 0.1, 0.2, \text{ and } 0.3$, as well as a pristine Bi_2SiO_5 ceramic. (Bottom panel) Reference patterns of monoclinic and tetragonal Bi_2SiO_5 .

wide compositional range, $x = 0.1\text{--}0.3$. This result is remarkable because in Bi_2SiO_5 ceramics doped only with La, ferroelectric and paraelectric phases coexist in a very narrow compositional range (only around La = 1 mol%).⁹ Additionally, the intensity of the diffraction peaks of the $\text{Bi}_4\text{Si}_3\text{O}_{12}$ secondary phase increases with the Ge content. This indicates that the incorporation of Ge promotes the thermal decomposition of Bi_2SiO_5 .

The XRD patterns of the samples were further analyzed *via* Rietveld refinement using a multiphase model consisting of the monoclinic and tetragonal Bi_2SiO_5 -type phases of along with the $\text{Bi}_4\text{Si}_3\text{O}_{12}$ and $\text{Bi}_{12}\text{Si}_{20}$ secondary phases. The analysis was conducted to determine the lattice parameters of the Bi_2SiO_5 phases and the mass fraction of each phase. Phases with diffraction intensities below the detection limit were excluded from the fitting model. The initial structural parameters of the Bi_2SiO_5 -type phases were derived from the relevant crystallographic data in the literature.^{10,12} The fitted XRD profiles and the refined parameters for each composition are shown in Fig. S1, Tables S1, and S2 in SI.

Fig. 3(a) shows the mass fraction of each phase, including the secondary phases of $\text{Bi}_4\text{Si}_3\text{O}_{12}$ and $\text{Bi}_{12}\text{Si}_{20}$, at different Ge contents (x). With the increase in Ge content (x) from 0 to 0.3, the fraction of the tetragonal Bi_2SiO_5 -type phase monotonically decreases from 100% to 36%, and that of the monocli-

**Fig. 3** (a) Mass fractions of Bi_2SiO_5 -type (monoclinic and tetragonal), $\text{Bi}_4\text{Si}_3\text{O}_{12}$ -type, and $\text{Bi}_{12}\text{Si}_{20}$ -type phases at different x ; (b) crystallite size of Bi_2SiO_5 -type (monoclinic and tetragonal) phases against x .

nic Bi_2SiO_5 -type phase increases from 0% to 53%. This indicates that the ratio of the tetragonal and monoclinic phases can be easily and widely tuned through the incorporation of Ge into La-substituted Bi_2SiO_5 . The Ge-substituted samples ($x = 0.1$ – 0.3) also contain $\text{Bi}_4\text{Si}_3\text{O}_{12}$ and $\text{Bi}_{12}\text{SiO}_{20}$ with a total mass fraction of approximately 10%. Although these secondary phases are difficult to completely remove from the Ge-substituted samples at this stage, their effects on the TCC of the resulting ceramics should be limited because of their small mass fractions and low dielectric permittivities ($\epsilon_r = 8.8$ for $\text{Bi}_4\text{Si}_3\text{O}_{12}$ and $\epsilon_r = 37.6$ for $\text{Bi}_{12}\text{SiO}_{20}$).^{21,22} Additionally, as shown in Table S2, the lattice volume of the tetragonal and monoclinic Bi_2SiO_5 -type phases tends to increase with the Ge content, confirming the incorporation of Ge into the Si site.

Fig. 3(b) shows the crystallite sizes of the tetragonal and monoclinic phases obtained from Rietveld refinement as functions of the Ge content. The crystallite size of the tetragonal phase is 95 nm at $x = 0$ and monotonically decreases with increasing x to 38 nm at $x = 0.3$. Conversely, the crystallite size of the monoclinic phase increases with x from 25 nm at $x = 0.1$ to 65 nm at $x = 0.3$. Interestingly, the sum of the crystallite sizes of the two phases is almost constant, approximately 100 nm. Fig. 4 shows the FE-SEM images of the fracture surfaces of the $(\text{Bi}_{0.97}\text{La}_{0.03})_2\text{Si}_{1-x}\text{Ge}_x\text{O}_5$ ceramics. Although the grain boundaries are not well defined, grains of several hundred nanometers are observed in the sample with $x = 0$. In contrast to the crystallite size, the grain size is less dependent on the Ge content. Thus, the structural characterization results shown above indicate that the samples co-substituted with La and Ge have intragranular-type nanocomposite structures with nanosized crystallites of the monoclinic phase formed in the matrix grains of the tetragonal phase.²³

Fig. 5(a) shows the temperature dependence of ϵ_r for the $(\text{Bi}_{0.97}\text{La}_{0.03})_2\text{Si}_{1-x}\text{Ge}_x\text{O}_5$ ceramics measured at 1 MHz over a wide temperature range, from -170 to 450 °C. As previously

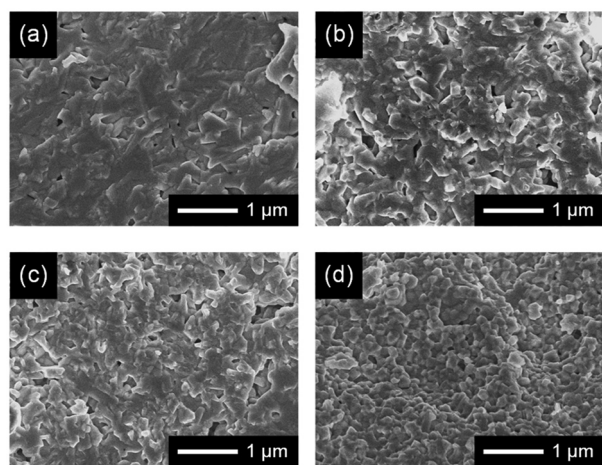


Fig. 4 FE-SEM images of the fracture surface of $(\text{Bi}_{0.97}\text{La}_{0.03})_2\text{Si}_{1-x}\text{Ge}_x\text{O}_5$ ceramics with x of (a) 0, (b) 0.1, (c) 0.2, and (d) 0.3.

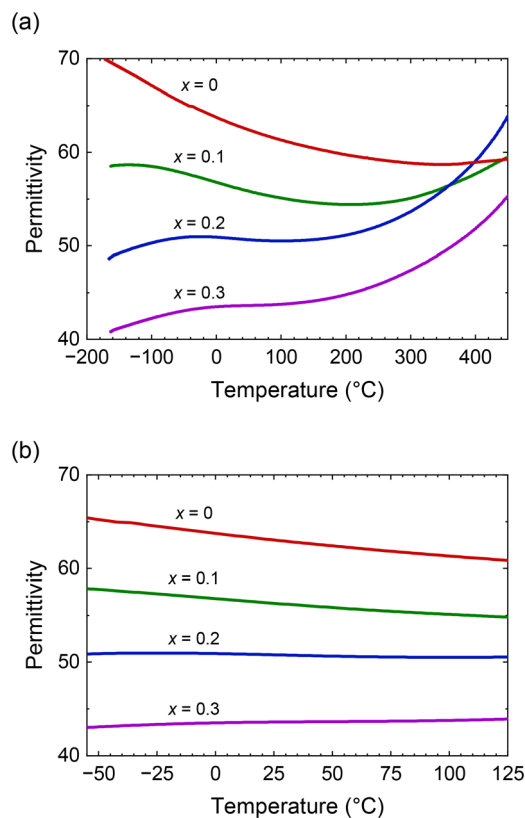


Fig. 5 (a) Temperature dependence of the dielectric permittivity for $(\text{Bi}_{0.97}\text{La}_{0.03})_2\text{Si}_{1-x}\text{Ge}_x\text{O}_5$ ceramics with $x = 0, 0.1, 0.2,$ and 0.3 in the temperature range of -170 to 450 °C. (b) Enlarged view of the dielectric permittivity in the temperature range from -55 to 125 °C.

reported, the curve for the sample without Ge ($x = 0$) exhibits a relatively large negative slope.⁹ As the Ge content increases, the slope gradually changes from negative to positive at temperatures below 200 °C. Additionally, ϵ_r of the co-substituted samples ($x = 0.1, 0.2,$ and 0.3) rapidly increases with temperature above 200 °C. The positive temperature dependence of ϵ_r in these samples at elevated temperatures is attributed to the ferroelectric phase transition of the monoclinic phase at T_C . The absence of a dielectric peak would be ascribed to the shift of the T_C of the monoclinic phase in these samples to above 450 °C because of the stabilization effect of the ferroelectric phase by the Ge substitution.¹⁷ In fact, the permittivity of a Bi_2GeO_5 glass-ceramic has also been reported to show no peak at temperatures up to 450 °C, suggesting that the T_C of Bi_2GeO_5 is substantially higher than that of Bi_2SiO_5 .²⁴ Fig. 5(b) compares the temperature stability of ϵ_r from -55 to 125 °C, which is the temperature range used to classify Class I MLCCs.¹ Notably, the samples with $x = 0.2$ and 0.3 show very stable permittivity in this temperature range. In particular, the sample with $x = 0.2$ exhibits $\epsilon_r > 50$ and superior temperature stability of ϵ_r .

To quantitatively evaluate the temperature stability of the dielectric permittivity, we calculated the TCC from the temperature dependence of capacitance using eqn (1) (Fig. 6). As



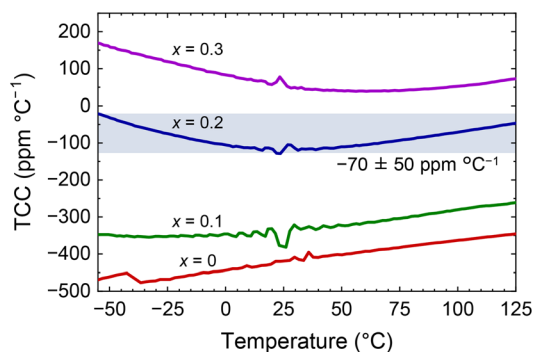


Fig. 6 Temperature dependence of TCC for $(\text{Bi}_{0.97}\text{La}_{0.03})_2\text{Si}_{1-x}\text{Ge}_x\text{O}_5$ ceramics with $x = 0, 0.1, 0.2,$ and 0.3 in the temperature range from -55 to 125 °C. The blue shaded area indicates the range of TCC variation in this temperature range for the $x = 0.2$ sample. The fluctuations in the TCC near room temperature were attributed to random errors in the measured capacitance.

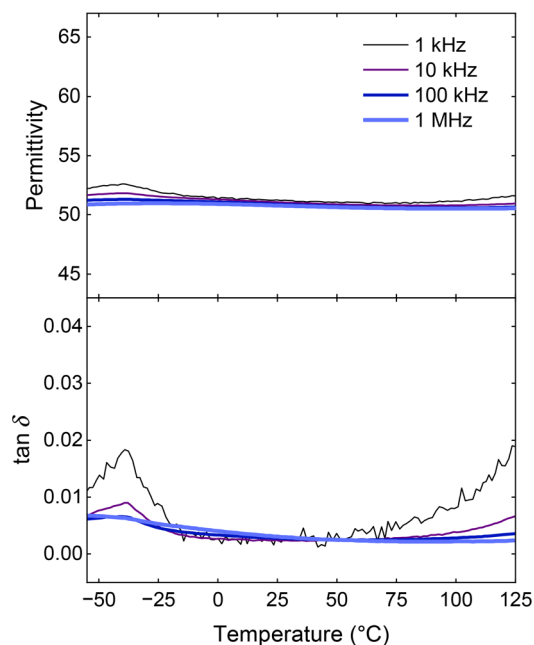


Fig. 7 Temperature dependences of the dielectric permittivity (top panel) and dielectric loss (bottom panel) for $(\text{Bi}_{0.97}\text{La}_{0.03})_2\text{Si}_{0.8}\text{Ge}_{0.2}\text{O}_5$, measured at 1 kHz– 1 MHz.

TCC is the slope of the capacitance *versus* temperature curve, the closer TCC is to 0, the weaker the temperature dependence. The sample without Ge ($x = 0$) exhibits a strongly negative TCC, between -350 ppm and -480 ppm °C $^{-1}$, over the entire temperature range. The increase in Ge content up to $x = 0.2$ pushes TCC closer to 0, with TCC becoming positive at $x = 0.3$. Among the samples tested herein, the sample with $x = 0.2$, which consists of almost equal amounts of the tetragonal and monoclinic phases, exhibits the best temperature stability, with TCC = -70 ± 50 ppm °C $^{-1}$ in the temperature range from -55 to 125 °C. Fig. 7 shows the temperature dependences of ϵ_r and $\tan \delta$ for the $x = 0.2$ sample (which showed the best dielectric performance) at frequencies of 1 kHz– 1 MHz. Data for all samples over the entire temperature range are shown in Fig. S2 in SI. The dielectric loss peak at -40 °C can be attributed to the dielectric relaxation of ice formed from water molecules absorbed in the pores of the samples.²⁵ Although the dielectric loss tends to increase at temperatures above 50 °C, it remains less than 0.02 even at 125 °C and the lowest frequency of 1 kHz. The observed dielectric loss is larger than that of CaZrO_3 -based materials, which is likely attributed to factors such as adsorbed water and oxide ion conduction. Therefore, further improvements in density and doping with aliovalent cations may help to reduce the dielectric loss. Additionally, ϵ_r does not considerably depend on the measurement frequency, confirming that the superior dielectric temperature stability of this sample is its intrinsic property than a result of extrinsic contributions such as electrical conduction.

Here, we discuss the formation process of the paraelectric-ferroelectric nanocomposite structure in $(\text{Bi}_{0.97}\text{La}_{0.03})_2\text{Si}_{1-x}\text{Ge}_x\text{O}_5$ ceramics, as well as the mechanism through which their dielectric temperature stability improves. To gain insight into the nanocomposite structure, we first prepared a powder with the composition of $x = 0.2$ using the same process as for the ceramic sample, but without pressing. The XRD measurement confirmed that the intensity ratio of the diffraction peaks from the tetragonal and monoclinic phases of the powder sample are similar

to those of the ceramic sample (Fig. S3 in SI). This suggests that the phase separation is not caused by mechanical effects related to the grain structure of ceramics. Then, we performed HAADF-STEM-EDS observations on ten different particles from the powder. Fig. 8 shows the HAADF-STEM-EDS elemental mapping of one representative particle, while the results for all particles are shown in Fig. S4 in SI. Since the crystalline sizes of the two phases, as determined by XRD, are both about 50 nm for this composition, regions of size about 50 nm separated by abrupt changes in composition should be observed if the phase separation occurs due to the nucleation and growth mechanism.²⁶ However, the results of the observation show that all constituent elements are uniformly distributed in each particle within the resolution range of the instrument, indicating that the nanocomposite structure has not formed through nucleation and growth. We believe that the phase separation in $(\text{Bi}_{0.97}\text{La}_{0.03})_2\text{Si}_{1-x}\text{Ge}_x\text{O}_5$ occurs *via* the spinodal decomposition mechanism, which is similar to that observed in the TiO_2 – SnO_2 and TiO_2 – VO_2 systems.^{27–29} However, since the spinodal decomposition is expected to be in its early stage after one hour of firing, the amplitude of the concentration fluctuations is small, making it difficult to detect using HAADF-STEM-EDS. A similar situation has been reported regarding the formation of lamellar-type phase separation structures in TiO_2 – VO_2 films.²⁷ To further understand the phase separation mechanism in $(\text{Bi}_{0.97}\text{La}_{0.03})_2\text{Si}_{1-x}\text{Ge}_x\text{O}_5$, it is important to observe the time evolution of the two-phase separation structure. However, extending the heat treatment time causes the Bi_2SiO_5 -type phases to decompose into the secondary phases, making this difficult at present.



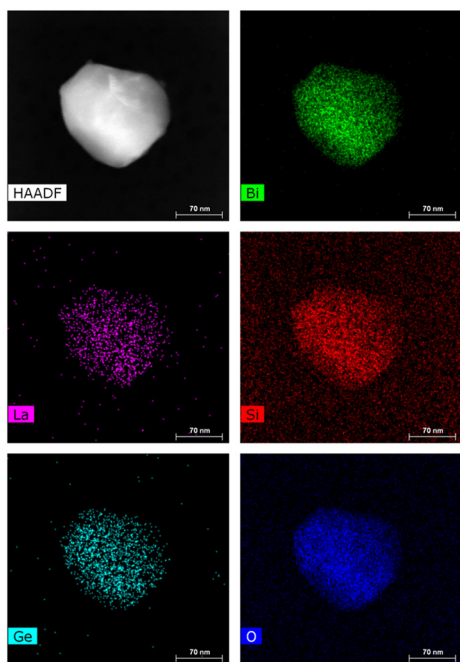


Fig. 8 HAADF-STEM-EDS elemental mapping of a $(\text{Bi}_{0.97}\text{La}_{0.03})_2\text{Si}_{0.8}\text{Ge}_{0.2}\text{O}_5$ particle.

Fig. 9 shows a schematic illustration of the mechanism for improving the dielectric temperature stability in $(\text{Bi}_{0.97}\text{La}_{0.03})_2\text{Si}_{1-x}\text{Ge}_x\text{O}_5$ ceramics. The sample without Ge ($x = 0$) consists of the single tetragonal (paraelectric) phase, which

shows a negative temperature dependence of ϵ_r . The incorporation of Ge results in the nucleation of the monoclinic (ferroelectric) phase with a positive temperature dependence of ϵ_r in the matrix of the tetragonal phase. The crystallite size of the monoclinic phase increases with the Ge content, leading to the spontaneous formation of a paraelectric–ferroelectric composite structure. The incorporation of Ge also shifts the T_C of the ferroelectric phase toward higher temperatures. The contents of the paraelectric and ferroelectric phases become almost equal at $x = 0.2$, resulting in the minimal temperature dependence of TCC $-70 \pm 50 \text{ ppm } ^\circ\text{C}^{-1}$ because of the opposite contributions of the two phases. As for the microstructures, it is unclear at this stage whether the small grain size or crystallite size of the samples obtained in this study affects the dielectric temperature stability. However, it is generally known that in ferroelectric ceramics, a reduction in grain size suppresses the development of ferroelectric order due to mechanical stress at grain boundaries, thereby broadening the temperature dependence of the dielectric permittivity.^{30–32} Therefore, it is possible that the small grain and crystallite sizes in this study also contribute to the improved temperature stability.

Although the achieved TCC of $-70 \pm 50 \text{ ppm } ^\circ\text{C}^{-1}$ does not meet the requirement for the C0G specification of MLCC, it is substantially smaller than that of conventional paraelectric ceramics such as TiO_2 ($-820 \text{ ppm } ^\circ\text{C}^{-1}$, $\epsilon_r = 114$ at 25°C) and CaTiO_3 ($-1442 \text{ ppm } ^\circ\text{C}^{-1}$, $\epsilon_r = 174$ at 25°C).^{33,34} In addition, the dielectric permittivity of the $x = 0.2$ sample ($\epsilon_r = 52$ at 25°C) is higher than that of CaZrO_3 ($\epsilon_r = 30$), which is used in

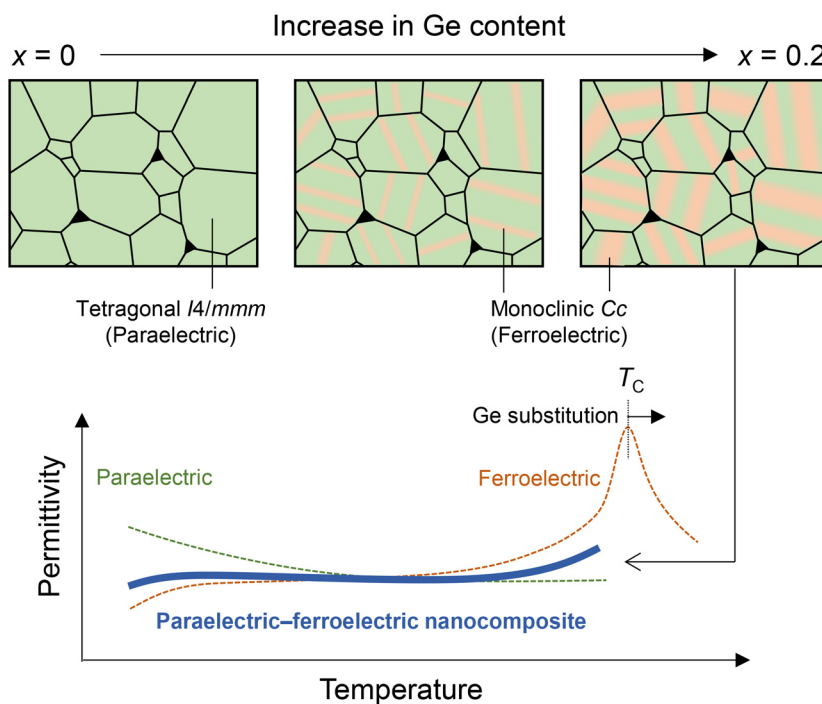


Fig. 9 Schematic of the mechanism for improving the dielectric temperature stability of $(\text{Bi}_{0.97}\text{La}_{0.03})_2\text{Si}_{1-x}\text{Ge}_x\text{O}_5$ ceramics. Note that the lamellar-type phase separation structure is not based on observed results, and other forms are also possible.



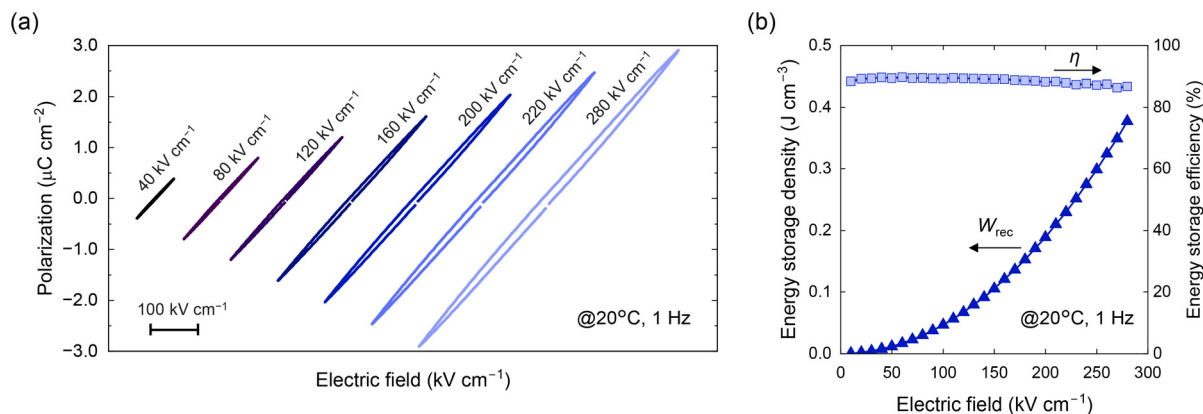


Fig. 10 (a) Bipolar P - E hysteresis loops and (b) energy storage properties of $(\text{Bi}_{0.97}\text{La}_{0.03})_2\text{Si}_{0.8}\text{Ge}_{0.2}\text{O}_5$ ceramics measured at different maximum electric fields (20–280 kV cm^{-1}).

the commercial C0G MLCCs.³⁵ It is also important to note that the samples prepared herein are not perfectly densified because of the difficulty of sintering. According to ref. 13, ϵ_r values of fully dense ceramics of monoclinic Bi_2SiO_5 and tetragonal $(\text{Bi}_{0.97}\text{La}_{0.03})_2\text{SiO}_5$, which were crystallized from corresponding glasses, are approximately 200 and 160 at room temperature, respectively—both significantly higher than that of the $x = 0.2$ sample fabricated in this study. Therefore, although further improvement in density is unlikely to reduce the TCC, it may lead to a significant increase in ϵ_r . Thus, we believe that Bi_2SiO_5 co-substituted with La and Ge shows great promise for applications in Class I MLCCs.

The direct measurement of the TCF values of the samples prepared in this study has not yet been carried out. However, based on the variable-temperature XRD data shown in ref. 13, the linear thermal expansion coefficients (α_L) near room temperature are reported to be 6.8 $\text{ppm } ^\circ\text{C}^{-1}$ for the monoclinic ferroelectric phase (pristine Bi_2SiO_5) and 9.8 $\text{ppm } ^\circ\text{C}^{-1}$ for the tetragonal paraelectric phase (La-substituted Bi_2SiO_5). Using these values and the volume fraction of the two phases [Fig. 3(a)], the linear thermal expansion coefficient of the $x = 0.2$ sample can be roughly estimated to be 8.0 $\text{ppm } ^\circ\text{C}^{-1}$ by applying the rule of mixtures. Accordingly, the temperature coefficient of resonant frequency (TCF) of this sample is estimated to be $\text{TCF} = -(\text{TCC} + \alpha_L)/2 = 31 \pm 25 \text{ ppm } ^\circ\text{C}^{-1}$, suggesting that it may also exhibit a favorable TCF as a microwave dielectric material.

Polarization response under high electric fields is also an important factor for MLCC applications. Fig. 10(a) shows the bipolar P - E curves of the sample with $x = 0.2$ measured at 20 $^\circ\text{C}$ and varying electric field amplitudes up to dielectric breakdown. Despite incomplete densification, the sample withstands electric fields up to 280 kV cm^{-1} . All P - E curves show linear behavior with a small hysteresis, probably because of leakage. In contrast to undoped Bi_2SiO_5 ceramics,^{10,11} no hysteresis associated with ferroelectric polarization switching is observed, even though this sample contains over 40% of the ferroelectric phase. Given the high T_C above 450 $^\circ\text{C}$ owing to

the Ge substitution, the absence of ferroelectric switching would be attributed to a high coercive field of the ferroelectric phase. Such a paraelectric-like linear polarization response is suitable for high-voltage applications because the effective ϵ_r of normal ferroelectrics is greatly reduced under bias voltages owing to ferroelectric polarization switching.^{36,37} We also calculated the recoverable energy storage density (W_{rec}) and energy storage efficiency (η) of this sample using the following equations:³⁸

$$W_{\text{rec}} = \int_{P_r}^{P_m} E dP \quad (2)$$

$$\eta = \frac{W_{\text{rec}}}{W_{\text{rec}} + W_{\text{loss}}} \quad (3)$$

where P_m , P_r , and W_{loss} are the maximum polarization, remanent polarization, and hysteresis loss, respectively. Fig. 10(b) shows the electric field dependence of W_{rec} and η . Owing to the linear polarization response of the sample, W_{rec} quadratically increases with the field strength, reaching 0.38 J cm^{-3} before the dielectric breakdown, while maintaining η values over 85% even at the maximum electric field. The obtained W_{rec} value is higher than those of undoped Bi_2SiO_5 ($W_{\text{rec}} = 0.06 \text{ J cm}^{-3}$) and La-substituted Bi_2SiO_5 ($W_{\text{rec}} = 0.29 \text{ J cm}^{-3}$).¹¹ Thus, this result also suggests that the co-substitution with La and Ge is a promising strategy for improving the dielectric properties of Bi_2SiO_5 ceramics.

Conclusions

Bi_2SiO_5 ceramics co-substituted with La and Ge, with the compositions of $(\text{Bi}_{0.97}\text{La}_{0.03})_2\text{Si}_{1-x}\text{Ge}_x\text{O}_5$ ($x = 0-0.3$), were prepared *via* the sol-gel process. We found that Ge^{4+} ions at the Si^{4+} site stabilize the ferroelectric phase and increase its T_C , whereas La^{3+} ions at the Bi^{3+} site break the long-range ferroelectric order, leading to the spontaneous formation of ferroelectric-paraelectric composites with a crystallite size below 100 nm at



$x = 0.1$ – 0.3 . The co-substitution with La and Ge substantially improved the dielectric stability of Bi_2SiO_5 ceramics because of the canceling out of the positive and negative temperature dependences of the ferroelectric and paraelectric phases, respectively. The ceramics with $x = 0.2$ showed the best temperature stability of -70 ± 50 ppm $^\circ\text{C}^{-1}$ with $\epsilon_r > 50$ as well as the high dielectric breakdown strength of 280 kV cm^{-1} and highly linear polarization response. As we could not attain complete densification of the prepared samples, further investigations of the densification process are needed to pave the way for the transfer of this material into practical applications.

Author contributions

Yoji Yasumoto: investigation, writing – original draft. Taro Kuwano: investigation. Hiroki Taniguchi: conceptualization, funding acquisition. Shinobu Fujihara: project administration, supervision. Manabu Hagiwara: conceptualization, investigation, funding acquisition, writing – review & editing, project administration, supervision.

Conflicts of interest

There are no conflicts to declare.

Data availability

The data that support the findings of this study are available within the article and its SI. Additional raw data are available from the corresponding author, Manabu Hagiwara, upon reasonable request.

Rietveld refinement results; Dielectric properties; XRD patterns; HAADF-STEM-EDS elemental mapping. See DOI: <https://doi.org/10.1039/d5dt01380a>

Acknowledgements

This work was supported by MEXT-Program for Creation of Innovative Core Technology for Power Electronics (Grant No. JPJ009777) and JSPS Grants-in-Aid for Transformative Research Areas (A) “Hyper-Ordered Structures Sciences” (Grant No. 20H05879 and 23H04119).

References

- M.-J. Pan and C. A. Randall, *IEEE Electr. Insul. Mag.*, 2010, **26**, 44–50.
- I. M. Reaney and D. Iddles, *J. Am. Ceram. Soc.*, 2006, **89**, 2063–2072.
- G. Wang, Z. Lu, Y. Li, L. Li, H. Ji, A. Feteira, D. Zhou, D. Wang, S. Zhang and I. M. Reaney, *Chem. Rev.*, 2021, **121**, 6124–6172.
- D. Zhou, L.-X. Pang, D.-W. Wang, C. Li, B.-B. Jin and I. M. Reaney, *J. Mater. Chem. C*, 2017, **5**, 10094–10098.
- W. Jia, Y. Hou, M. Zheng, Y. Xu, M. Zhu, K. Yang, H. Cheng, S. Sun and J. Xing, *IET Nanodielectr.*, 2018, **1**, 3–16.
- M. T. Sebastian, R. Uvic and H. Jantunen, *Int. Mater. Rev.*, 2015, **60**, 392–412.
- M. T. Sebastian, H. Wang and H. Jantunen, *Curr. Opin. Solid State Mater. Sci.*, 2016, **20**, 151–170.
- H. Yu, J. Liu, W. Zhang and S. Zhang, *J. Mater. Sci.: Mater. Electron.*, 2015, **26**, 9414–9423.
- Y. Yasumoto, T. Kuwano, H. Taniguchi, S. Fujihara and M. Hagiwara, *ACS Appl. Electron. Mater.*, 2023, **5**, 4323–4329.
- H. Taniguchi, A. Kuwabara, J. Kim, Y. Kim, H. Moriwake, S. Kim, T. Hoshiyama, T. Koyama, S. Mori, M. Takata, H. Hosono, Y. Inaguma and M. Itoh, *Angew. Chem., Int. Ed.*, 2013, **52**, 8088–8092.
- K. Sakamoto, M. Hagiwara, H. Taniguchi and S. Fujihara, *J. Mater. Sci.*, 2021, **56**, 8415–8426.
- S. Georges, F. Goutenoire and P. Lacorre, *J. Solid State Chem.*, 2006, **179**, 4020–4028.
- H. Taniguchi, S. Tatewaki, S. Yasui, Y. Fujii, J. Yamaura and I. Terasaki, *Phys. Rev. Mater.*, 2018, **2**, 045603.
- K. P. Surendran, N. Santha, P. Mohanan and M. T. Sebastian, *Eur. Phys. J. B*, 2004, **41**, 301–306.
- Y. T. Fei, S. J. Fan, R. Y. Sun, J. Y. Xu and M. Ishii, *J. Mater. Sci. Lett.*, 2000, **19**, 893–895.
- B. Jancar, D. Suvorov, M. Valant and G. Drazic, *J. Eur. Ceram. Soc.*, 2003, **23**, 1391–1400.
- J. Park, B. G. Kim, S. Mori and T. Oguchi, *J. Solid State Chem.*, 2016, **235**, 68–75.
- F. Izumi and K. Momma, *Solid State Phenomena*, 2007, **130**, 15–20.
- S. A. Hassanzadeh-Tabrizi, *J. Alloys Compd.*, 2023, **968**, 171914.
- V. P. Zhareb and V. M. Skorikov, *Inorg. Mater.*, 2003, **39**, S121–S145.
- H. Xie, F. Li, H. Xi and D. Zhou, *Trans. Indian Ceram. Soc.*, 2015, **74**, 83–85.
- M. Valant and D. Suvorov, *J. Am. Ceram. Soc.*, 2001, **84**, 2900–2904.
- K. Niihara, *J. Ceram. Soc. Jpn.*, 1991, **99**, 974–982.
- S. Panyata, S. Eitssayeam, G. Rujijjanagul, T. Tunkasiri, A. Munpakdee and K. Pengpat, *Integr. Ferroelectr.*, 2019, **195**, 187–195.
- A. Angulo-Sherman and H. Mercado-Urbe, *Phys. Rev. E: Stat., Nonlinear, Soft Matter Phys.*, 2014, **89**, 022406.
- F. Findik, *Mater. Des.*, 2012, **42**, 131–146.
- G. Sun, X. Cao, Y. Yue, X. Gao, S. Long, N. Li, R. Li, H. Luo and P. Jin, *Sci. Rep.*, 2018, **8**, 5342.
- Z. Hiroi, H. Hayamizu, T. Yoshida, Y. Muraoka, Y. Okamoto, J. Yamaura and Y. Ueda, *Chem. Mater.*, 2013, **25**, 2202–2210.



- 29 M. Park, T. E. Mitchell and A. H. Heuer, *J. Am. Ceram. Soc.*, 1975, **58**, 43–47.
- 30 T. Hoshina, T. Furuta, T. Yamazaki, H. Takeda and T. Tsurumi, *Jpn. J. Appl. Phys.*, 2012, **51**, 09LC054.
- 31 M. Hagiwara and S. Fujihara, *Appl. Phys. Lett.*, 2015, **107**, 012903.
- 32 M. Hagiwara and S. Fujihara, *Jpn. J. Appl. Phys.*, 2015, **54**, 10ND10.
- 33 L. J. Berberich and M. E. Bell, *J. Appl. Phys.*, 1940, **11**, 681–692.
- 34 Y. Saito, H. Takao and K. Wada, *Ceram. Int.*, 2008, **34**, 745–751.
- 35 I. Levin, T. G. Amos, S. M. Bell, L. Farber, T. A. Vanderah, R. S. Roth and B. H. Toby, *J. Solid State Chem.*, 2003, **175**, 170–181.
- 36 G. Yang, Z. Yue, J. Zhao, H. Wen, X. Wang and L. Li, *J. Phys. D:Appl. Phys.*, 2006, **39**, 3702–3707.
- 37 Z. Li, S. Yan, J. Xia, F. Cao, X. Chen, Y. Song, Y. Chen, Z.-S. Lin and G. Wang, *Ceram. Int.*, 2022, **48**, 27439–27447.
- 38 Z. Yang, H. Du, L. Jin and D. Poelman, *J. Mater. Chem. A*, 2021, **9**, 18026–18085.

